Supplementary Information for

An ecophysiological explanation for manganese enrichment in rock varnish

Usha F. Lingappa*, Chris M. Yeager, Ajay Sharma, Nina L. Lanza, Demosthenes P. Morales, Gary Xie, Ashley D. Atencio, Grayson L. Chadwick, Danielle R. Monteverde, John S. Magyar, Samuel M. Webb, Joan Selverstone Valentine, Brian M. Hoffman, Woodward W. Fischer

* Correspondence: usha@caltech.edu

This PDF file includes:

B

location	rock type collected	GPS coordinates	elevation (m)	average temp. (°C)	average rainfall (mm/year)
Barstow, CA	rhyolite	34°37'44.3"N 116°57'05.0"W	676	18.4	134
Babbitt Ranch, AZ	basalt, sandstone	35°40'59.9"N 111°24'13.3"W	1281	15.1	141
Black Canyon, NM	rhyolite	33°59'7.802"N 106°58'41.413"W	1656	13.7	260
Mesa Prieta, NM	basalt	36°8'13.099"N 106°1'20.129"W	1781	10.75	260
White Rock, NM	tuff	35°48'24.848"N 106°12'1.734"W	1845	9.1	479
Green River, UT	sandstone, conglomerate	38°52'50.094"N 110°12'23.797"W	1291	12	180
Basin, WY	sandstone	44°24'25.214"N 108°6'23.797"W	1224	7.6	175

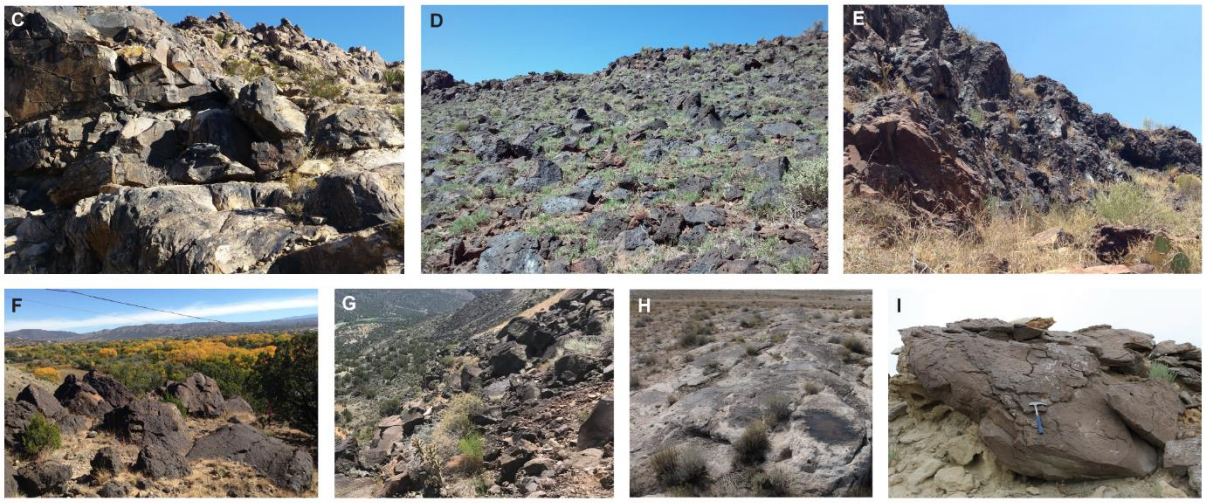

Figure S1: Field areas in this study. (*A*) Map of the western United States, with varnish sampling locations indicated. (*B*) Field area metadata. Average temperature and rainfall from nearest weather station on US Climate Data. (*C*-*I*) Context photos showing varnish from Barstow (*C*), Babbitt Ranch (*D*), Black Canyon (*E*), Mesa Prieta (*F*), White Rock (*G*), Green River (*H*), and Basin (*I*) sampling locations.

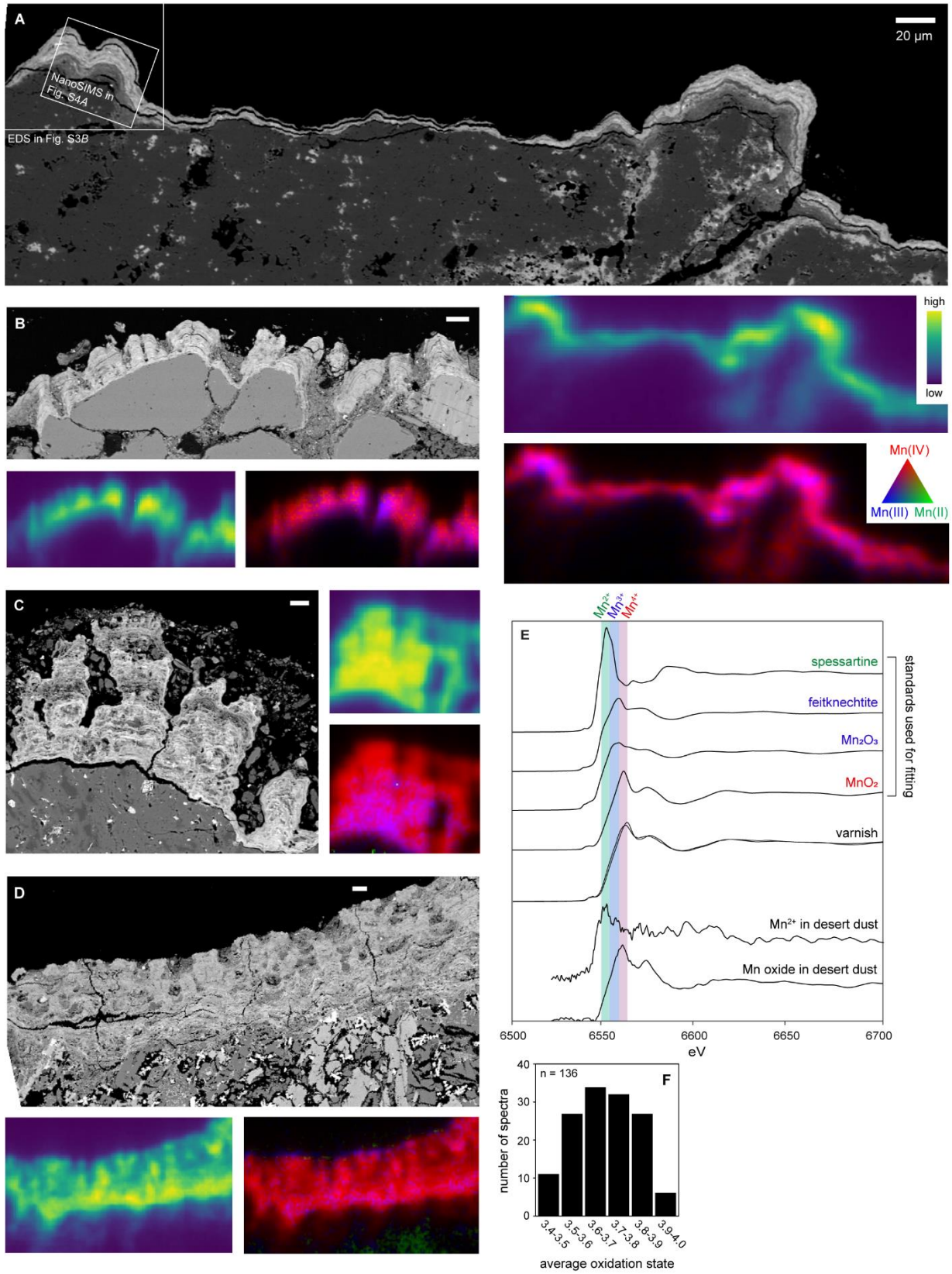

Figure S2: Extended SEM and synchrotron data. (*A-D*) Additional examples of SEM images

showing accretionary laminations with stromatolitic textures and manganese K-edge maps showing manganese distribution and redox heterogeneity in varnish thin sections. (*A*) Rhyolite from Black Canyon, NM. (*B*) Sandstone from Babbitt Ranch, AZ. (*C*) Rhyolite from Black Canyon, NM. (*D*) Basalt from Mesa Prieta, NM. (*E*) Manganese K-edge XANES spectra. For standards we employed spectra from spessartine for Mn^{2+}, both feitknechtite (β-MnOOH) and Mn_2O_3 as options for Mn^{3+}, and an internal endmember for Mn^{4+}. The two varnish spectra shown here plotted on top of each other represent the first and third quartile of our varnish dataset, with average oxidation states of 3.6 and 3.8 respectively. The desert dust spectra demonstrate the presence of manganese oxides in addition to trace igneous Mn^{2+} in surrounding dust that supplies the source of the material for varnish formation. (*F*) Histogram showing distribution of manganese redox states of all varnish spectra collected, including basalt, rhyolite, and sandstone samples.

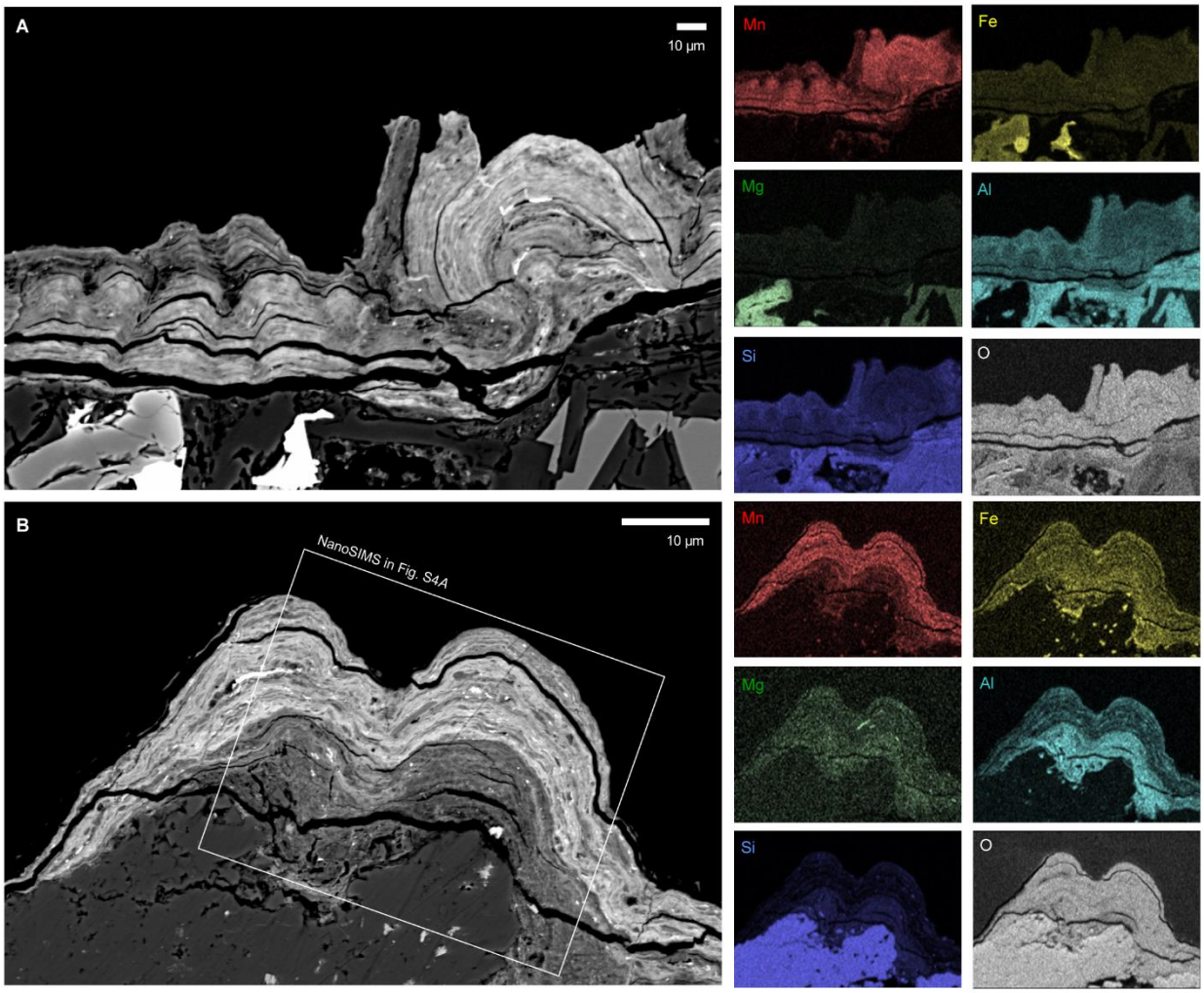

Figure S3: Backscatter SEM images with EDS chemical maps showing the distribution of major elements in varnish and underlying rock. (*A*) A mafic example, basalt from Babbitt Ranch, AZ; the sample shown in Fig. 1. (*B*) A felsic example, rhyolite from Black Canyon, NM; the sample shown in Fig. S2*A*. Varnish is comprised primarily of manganese and iron oxides (reflected in the Mn and Fe channels, respectively) and clay minerals (reflected in the Si, Al, and Mg channels). Detrital grains are embedded in the laminated cement. The high manganese content occurs in the cement itself, not the detrital grains.

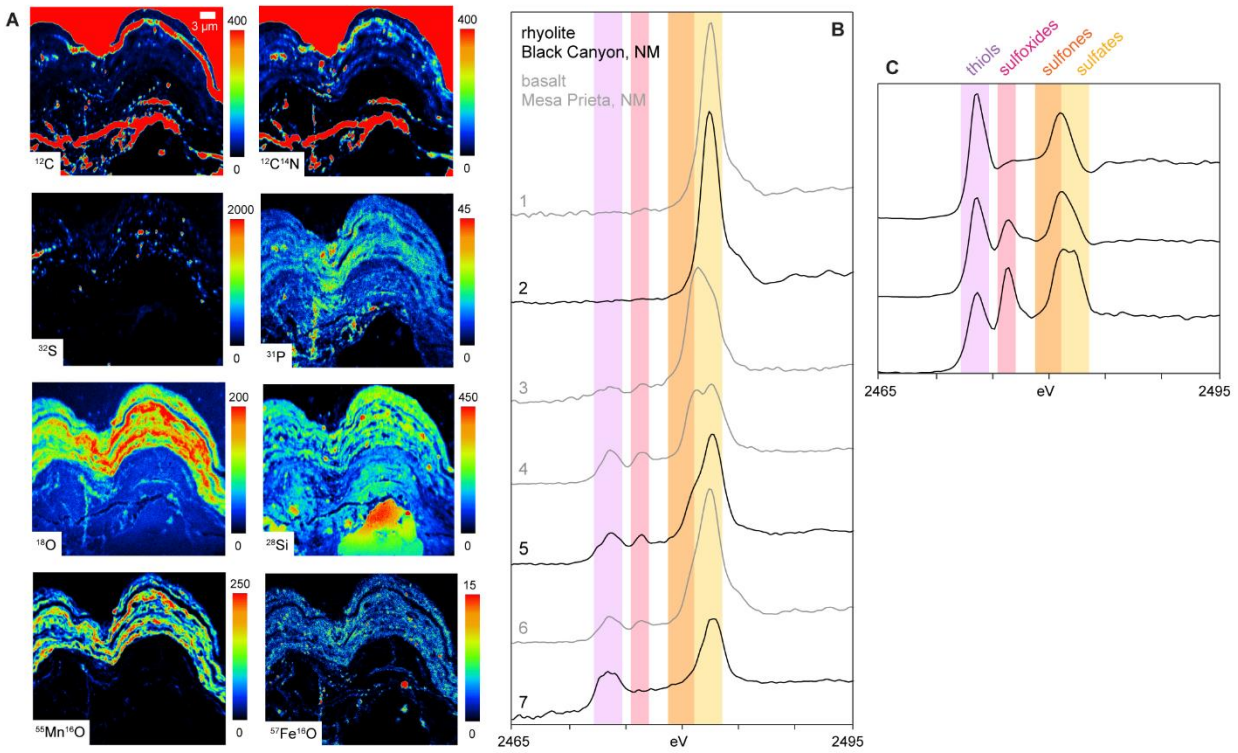

Figure S4: Sulfur distribution and speciation as a biosignature in varnish. (*A*) NanoSIMS images of the sample shown in Figs. S2*A* and S3*B*, to visualize the distribution of lighter elements indicative of biomass. Of the major biological elements, carbon and nitrogen signals are overwhelmed by background resin, but the resin is extremely poor in sulfur content; that, plus the high ion-yield of organic matter enables ^{32}S ion images to provide a measure of organic matter native to the varnish. (*B*) Sulfur K-edge XANES spectra from two varnish thin sections. These spectra demonstrate complex sulfur speciation in varnish, with both oxidized and reduced organic species that are consistent with biological material, in addition to sulfate salts. (*C*) Sulfur K-edge spectra taken on *Chroococcidiopsis* cells, representing the dominant source of biomass in varnish, exhibit the same organic sulfur moieties we observed in varnish.

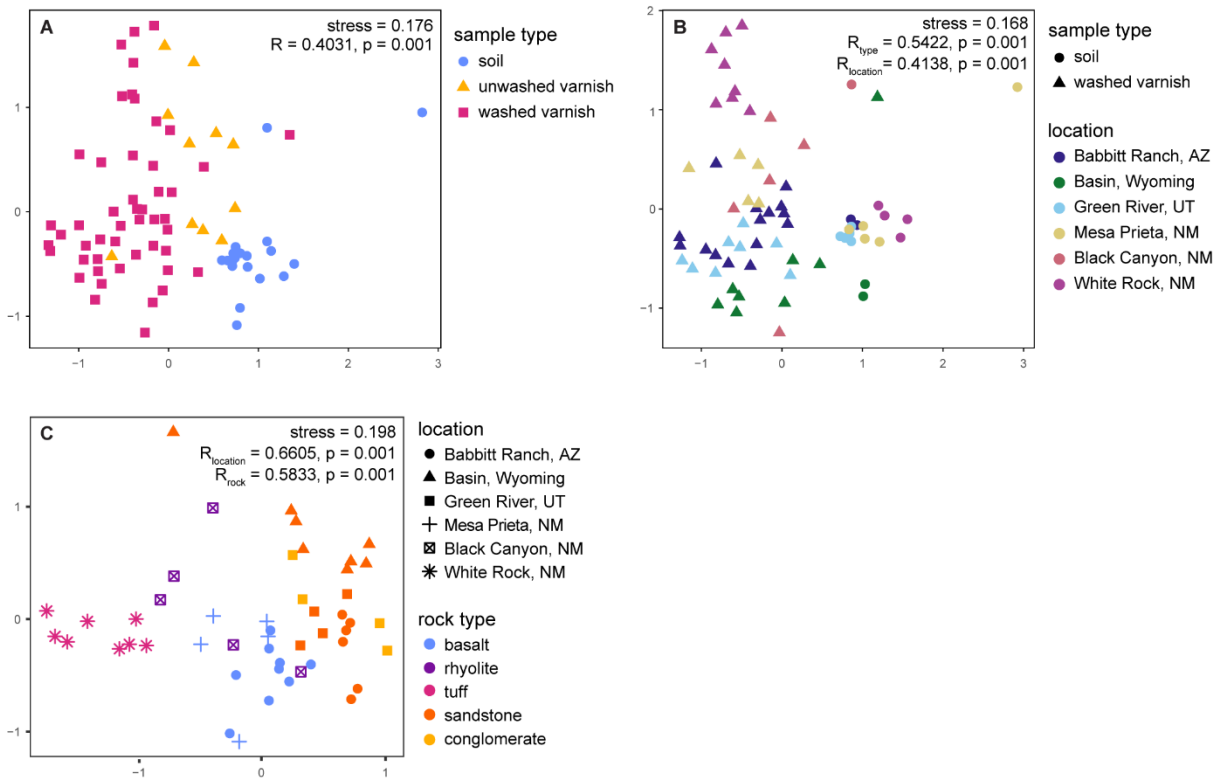

Figure S5: Nonmetric multidimentional scaling (NMDS) ordination analyses of 16S rRNA gene amplicon data to visualize variance. Each point represents the microbial community recovered from a sample; relative proximity between points indicates their similarity. (*A*) The varnish microbial community is distinct from that in surrounding soils, regardless of sample location or rock type. Rinsing the varnished rocks with sterile water to remove surficial dust further increased NMDS separation between varnish and soils. Thus, the remainder of our DNA analyses focused on washed varnish samples, to more accurately target taxa endemic to varnish. The analysis of similarities (ANOSIM) statistic *R* for soil vs. unwashed varnish = 0.4265, p = 0.001; and soil vs. washed varnish = 0.5442, p = 0.001. (*B*) Washed varnish and surrounding soil samples colored by sample location. (*C*) Washed varnish samples alone, colored by rock type. Among varnish samples, we observed some higher order clustering based on rock type and location.

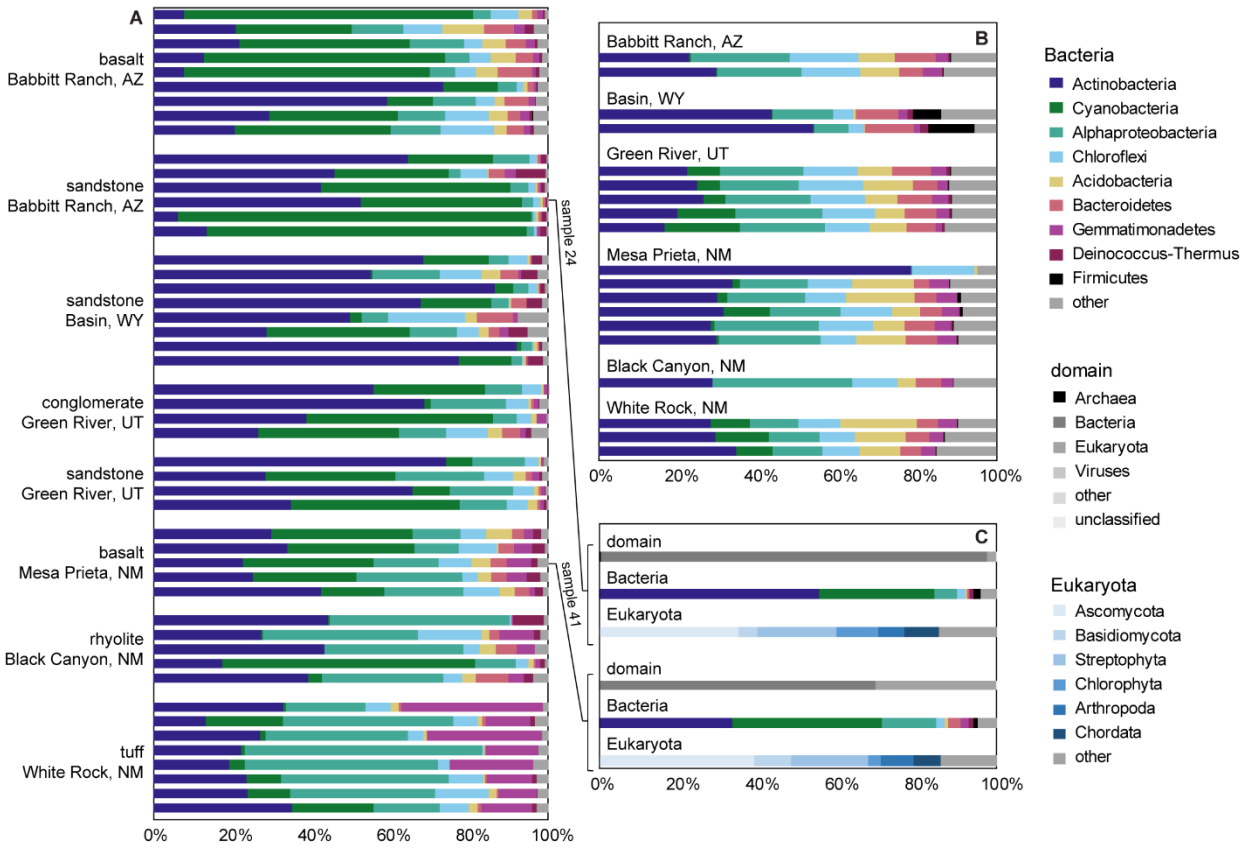

Figure S6: Phylum level community composition of (*A*) varnish 16S rRNA gene amplicon reads, (*B*) surrounding desert soil 16S rRNA gene amplicon reads, and (*C*) varnish shotgun metagenome reads. The varnish community is dominated by bacteria, with eukaryotes comprising 2.4% and 30.5%, and archaea comprising <0.5% of metagenome reads.

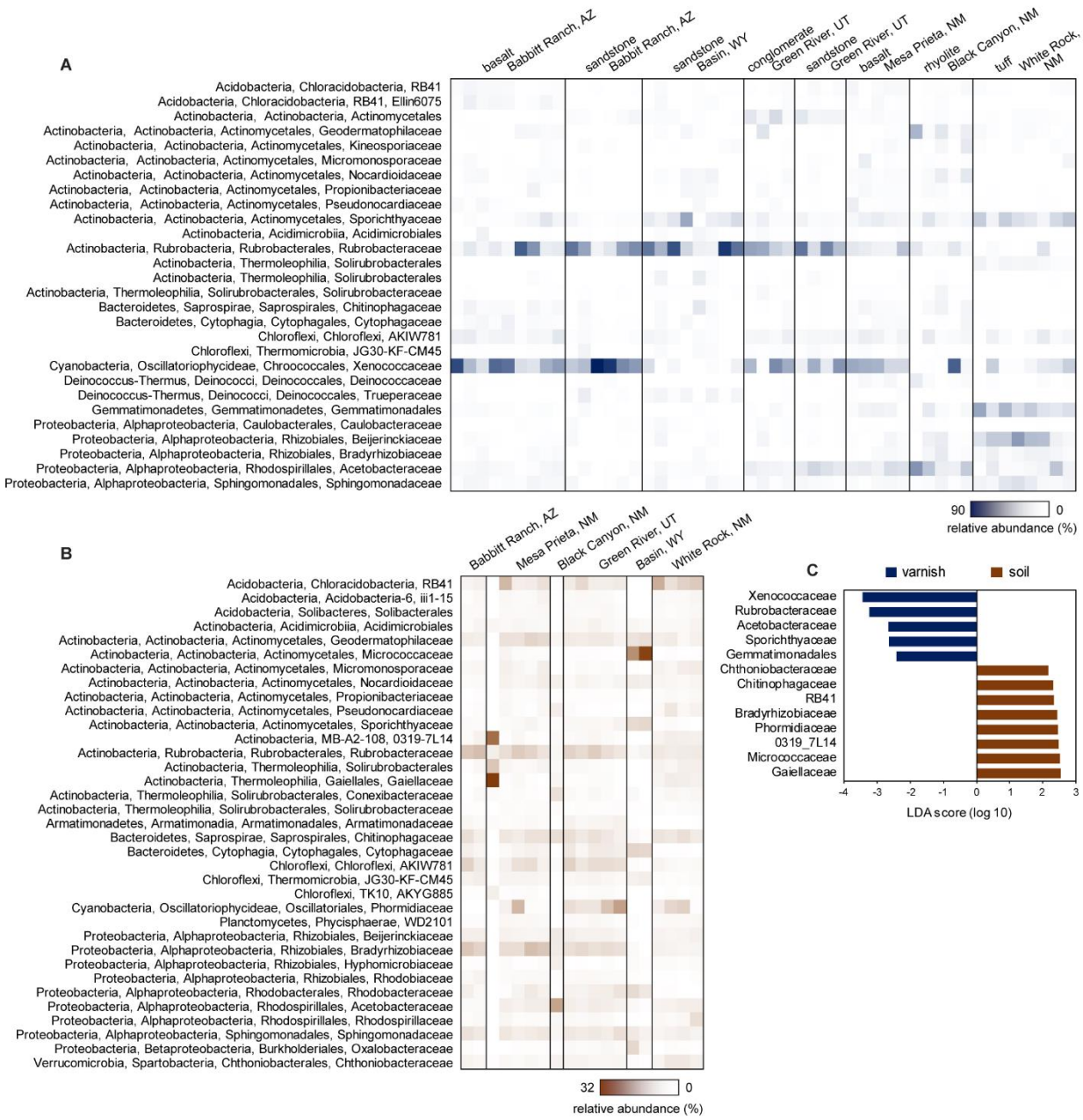

Figure S7: Major families characterizing the varnish microbial community. (*A-B*) The most abundant families (average relative abundance > 0.5%) identified in 16S rRNA gene amplicon reads from varnish (*A*) and surrounding desert soils (*B*). (*C*) Linear discriminant analysis effect size (LEfSe) identifying families that contributed most strongly to the distinction between the microbial communities of varnish vs. soil. The family Xenococcaceae was a major constituent of the varnish microbial community across all rock types and locations examined, and was the strongest contributor identified by LEfSe as characterizing varnish relative to soil.

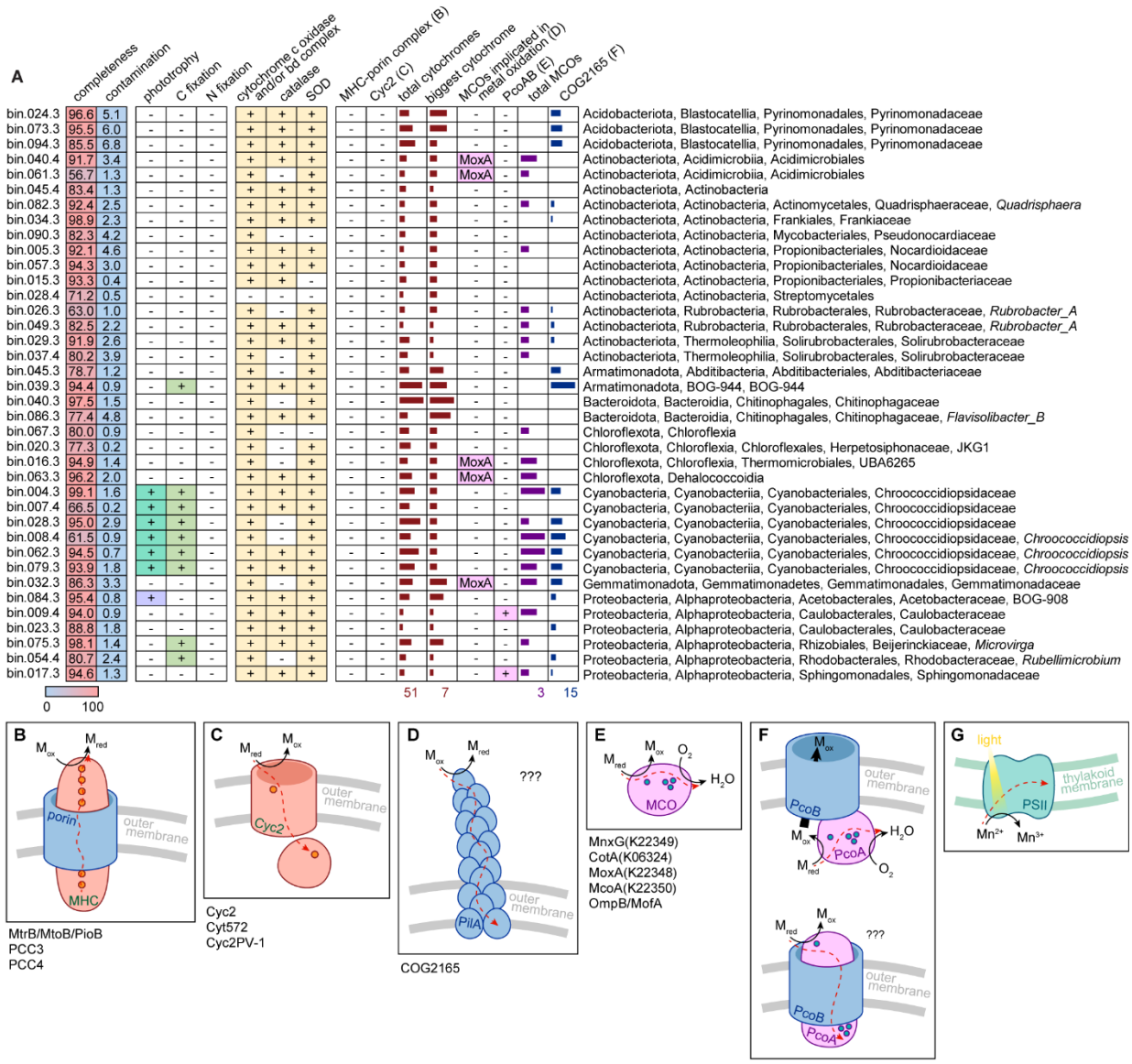

Figure S8: Metagenomic insights into varnish ecology. (*A*) We recovered 38 high quality MAGs from varnish shotgun metagenomes, 6 of which belonged to the Chroococcidiopsidaceae. Genes indicative of autotrophy are highlighted in green, showing that the Chroococcidiopsidaceae are the main primary producers and therefore keystone members of the ecosystem. Genes indicative of interactions with O_2 and reactive oxygen species (heme-copper O_2 reductase and/or *bd* O_2 reductases, catalase, and superoxide dismutase) are highlighted in yellow, demonstrating the strikingly aerobic nature of this ecosystem. Genes implicated in metal cycling processes, including MHC-porin complexes (*B*), Cyc2 homologs (*C*), high-potential MCOs (*D*), putative MCO-porin complexes (*E*), the COG2165 pilin system (*F*), and photosystem II (*G*), were also catalogued, along with counts of total cytochromes, largest MHC, and total MCOs in each genome bin. Dashed red arrows indicate electron flow.

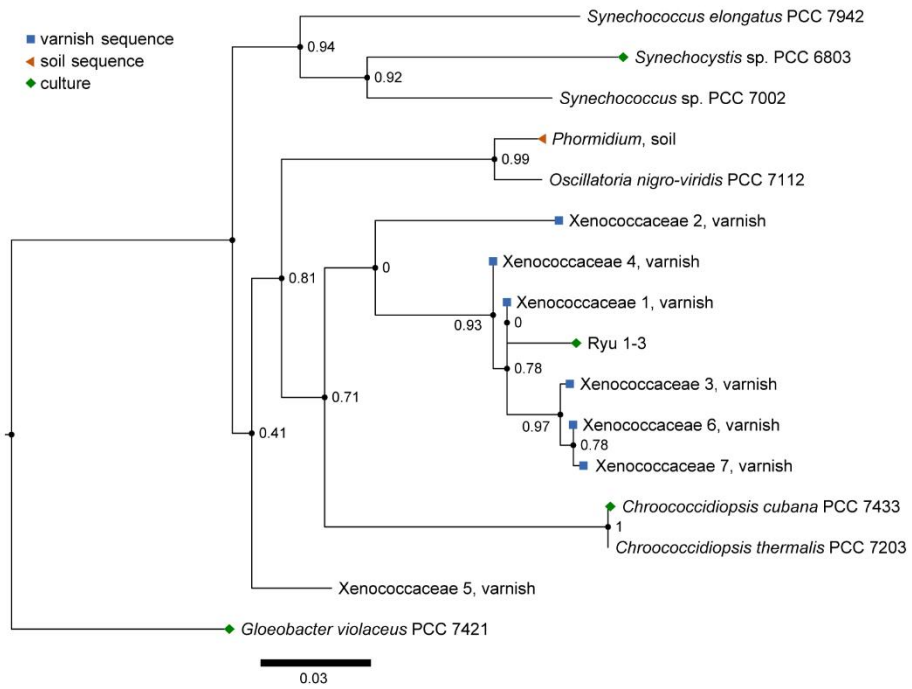

Figure S9: Phylogenetic tree showing relationships between the Cyanobacteria examined in this study. Tree includes cultured strains we used to investigate intracellular manganese accumulation and speciation (model organism *Synechocystis* sp. PCC 6803, *Chroococcidiopsis* strains Ryu 1-3 and PCC 7433, and the deep branching *Gloeobacter violaceous* PCC 7421), along with the most abundant 16S sequences recovered from varnish and soil (Xenococcaceae and Phormidium, respectively).

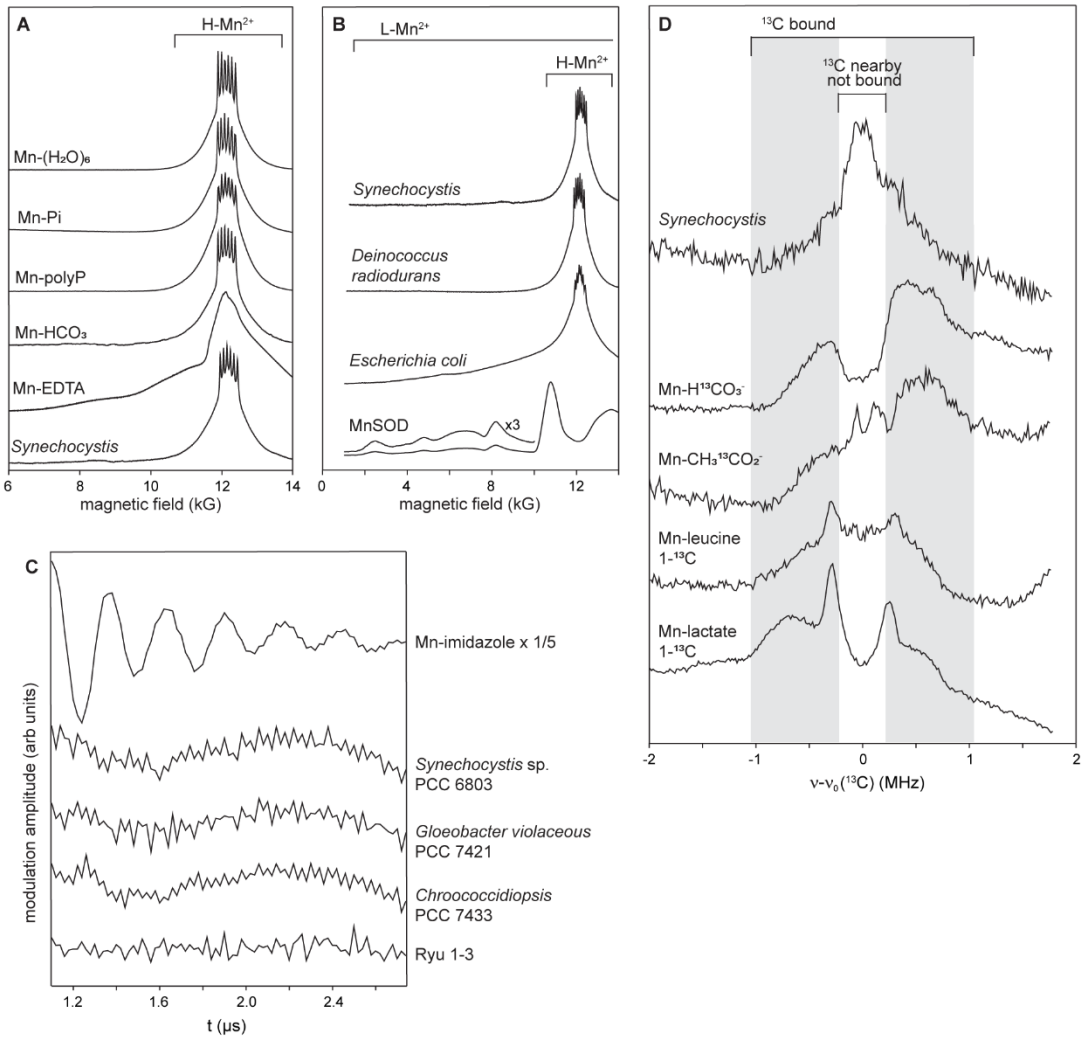

Figure S10: Additional paramagnetic resonance data. (*A-B*) Absorption display CW EPR spectra. The frozen solution EPR spectra of Mn-$(H_2O)_6$, Mn-HCO_3, Mn-Pi, and Mn-polyP are representative exemplars for H-Mn^{2+} complexes with six sharp peaks (Mn^{2+} hyperfine lines) riding on a ~4 kG 'skirt'. Both *Deinococcus radiodurans* and all of our cyanobacterial strains (*Synechocystis* included as representative example) displayed cellular Mn EPR spectra indicative of this type of manganese speciation. In contrast, L-Mn^{2+}, including strongly chelated (e.g. Mn-EDTA) and protein-bound (e.g. MnSOD) Mn^{2+} display spectra which go well beyond the "H" 4 kG skirt, both at low and high magnetic fields. In *Escherichia coli*, the much broader skirt around the Mn^{2+} hyperfine lines relative to *Deinococcus* and *Synechocystis* indicates significantly more manganese bound to strongly chelating ligands or proteins. (*C*) 3-pulse ESEEM timewaves, which show modulations arising from ^{14}N hyperfine coupling, as observed in a frozen solution of Mn-imidazole. None of the cyanobacterial strains examined here displayed ^{14}N modulation, indicating a negligible population of nitrogenous ligands in the manganese environment. (*D*) ^{13}C Mims ENDOR, characterizing Mn-^{13}C coupling in ^{13}C-labelled *Synechocystis*. The region centered around the ^{13}C Larmor frequency shown with two gray stripes (denoted as "^{13}C bound") is similar to that observed for standard Mn^{2+} complexes with ^{13}C-labelled bicarbonates and organic molecules, and is indicative of manganese bound to

carboxylate ligands. The high central peak at the ^{13}C Larmor frequency (denoted "^{13}C nearby, not bound") arises from the nearby ^{13}C nuclei that are not coordinated to manganese, suggesting that these ligands might be multi-C molecules such as small organic acids.

Supplemental Text

A. Building on previous hypotheses of varnish formation

Varnish genesis is the topic of a substantial body of previous work, which has shed important light on a wide range of sedimentary, geochemical, and biological factors. Analyses of accretionary microtextures (1–3) and trace element and isotopic compositions (4–7) demonstrated that the material comprising varnish originates from dust external to the host rock, mediated by atmospheric precipitation. Other studies examined the importance of silica in the varnish material, proposing processes of silica dissolution, gelling, condensing, and hardening as controlling the development of such rock coatings (8, 9). The presence of biology in varnish has been documented by various techniques including culturing (10, 11), DNA analyses (10, 12–16), and SEM imaging of filamentous and coccoidal forms (2, 10, 17); and a role for microbes in binding together the oxides and clay minerals that comprise varnish has been suggested (18).

Several different mechanisms for the enrichment and oxidation of manganese have been proposed; this includes both biological and abiotic processes. Hypotheses attributing the manganese in varnish to biological activity generally invoke microbial manganese oxidation (10, 11, 19–22). Model organisms like *Bacillus* sp. SG-1 and *Pseudomonas putida* MnB-1 strains are known to oxidize Mn^{2+} extracellularly (Fig. S8*E*)—generating manganese oxides that accumulate on their exosporia or glycocalyx, respectively (23). Previous studies have isolated similar bacteria from varnish (10, 11), and suggested that manganese oxide encrusted microbes could provide the manganese source for the varnish cement (18). Fungi are also known to oxidize manganese (24, 25), and have similarly been implicated in varnish (20, 26). In contrast, abiotic models of varnish formation have advocated thermodynamic arguments for the preferential mobility of manganese at certain pH regimes, enabling the enrichment of manganese

from dust deposited on the rock surface through water leaching (7). The abiotic oxidation of manganese can be catalyzed by either mineral surface coordination (27) or photochemistry (28), both of which have been invoked in varnish hypotheses. Many of these processes could contribute to varnish accretion and manganese oxidation, however, none of them entirely explain the high concentrations and specific enrichment of manganese in this material.

It has been argued that the very slow rate of varnish formation rules out mechanisms based on biological processes that are known from laboratory experiments to proceed at more rapid rates (7, 18, 29). However, it is important to note that rates of microbial activities under idealized laboratory conditions are not necessarily representative of the natural environment (30). Most cells in the environment are not actively growing exponentially most of the time. Especially in harsh environments, such as those relevant to varnish formation. In this context microbial growth can be very slow, and limited by water availability or nutrient availability, or inhibited by excessive heat or radiation. The relatively rapid growth rates we can sometimes achieve in the laboratory enable us to study processes that might otherwise happen too slowly to capture on experimental timescales—but this has very little bearing on how quickly such processes might be occurring in the environment.

B. Genomic insights into manganese cycling in the varnish ecosystem

Our synchrotron data indicated that manganese redox cycling (both oxidation and reduction) not only contributes to the formation of varnish, it continues in well-developed varnish—hinting that the varnish is characterized by unique opportunities for biology to interface with manganese redox cycling. Biological processes can catalyze both reductions and oxidations of manganese. In order to better understand which manganese redox reactions might be mediated

by varnish community members, we searched for genomic hallmarks of known biological metal cycling processes in our varnish metagenomic datasets. This included both reactions that could be directly coupled to cellular energy conservation, and reactions catalyzed by enzymes but not directly involved in energy metabolism.

Coupling metabolic processes to redox reactions of insoluble, extracellular metal oxides requires the ability to transport electrons into or out of cells. This process has been best studied in the model systems for dissimilatory metal oxide reduction—*Shewanella* and *Geobacter*, that use large multiheme cytochromes (MHC) embedded in outer membrane beta barrel porins as conduits between their electron transport chains and extracellular electron acceptors (Fig. S8*B*) (31). A similar biochemical strategy for extracellular electron transfer (EET) has been identified in organisms with metabolisms based on both iron and manganese oxidation (32, 33). None of our varnish MAGs were phylogenetically associated with known EET capable organisms, however this trait is broadly distributed throughout many bacterial phyla. Therefore, we used a gene-centric method to assess EET capability—an approach similar to the strategy employed in a recent survey of neutrophilic iron oxidizer genomes (32). We specifically screened for the porin proteins from known MHC-porin complexes MtrB (*Shewanella oneidensis*) (34), MtoB (*Sideroxydans lithotrophicus*) (35), and PioB (*Rhodopseudomonas palustrus*) (36), along with PCC3 and PCC4, hypothetical porin-cytochrome complex gene clusters from other known iron oxidizers (32). We also screened more generally for any MHCs by counting the occurrence of heme binding domains (CxxCH motifs), and determined whether or not these fell within gene clusters that also contained predicted beta barrel porins. Notably, we did not detect any MHCs with greater than 10 hemes—a characteristic of many organisms capable of EET—and none of our predicted MHCs resided in porin-MHC gene clusters. This suggested that microbial

metabolisms based on EET via large MHCs are uncommon in varnish—far rarer than in soils and sediments.

The dearth of organisms exploiting the oxides in varnish for dissimilatory metal reduction is understandable given that varnish appears to be a thoroughly aerobic environment—O_2 will always be a better electron acceptor for respiration. Unlike the anaerobic sediment environments wherein dissimilatory metal reduction is an important biogeochemical process, varnish may present a habitat with different opportunities for metal cycling. In this setting, biological manganese reduction might be more likely to occur via processes aimed at mobilizing and assimilating manganese rather than for core energy metabolism.

Pili have been implicated in metal reduction in *Geobacter* (Fig. S8*D*), and a pilin system in Cyanobacteria—homologous to the one from *Geobacter*—has been proposed to allow *Synechocystis* sp. PCC 6803 to grow on manganese oxides as their sole manganese source, presumably via reductive dissolution (37). While the role of pili in metal reduction has been the topic of some controversy (38), it is worth noting the presence of these pilin proteins (COG2165) in several of our varnish MAGs, including 5 of the 6 Chroococcidiopsiaceae MAGs.

Not all known iron oxidizing organisms use large MHCs—another strategy for EET involves an outer membrane cytochrome with a single heme bound in the center of a beta barrel porin that transfers electrons from iron to other small periplasmic cytochromes (Fig. S8*C*). In principle, an analogous system can be imagined for manganese, though one has not as yet been identified. We used BLAST to search for the outer membrane cytochromes Cyc2 (*Acidothiobacillus ferrooxidans*) (39), Cyt572 (*Leptospirillum* spp.) (40), and Cyc2PV-1 (*Mariprofundus ferrooxydans* PV-1) (41), all distant homologs broadly found in iron oxidizers. No significant hits for these proteins were identified in any of our MAGs.

We also counted total putative *c*-type cytochrome encoding genes in each MAG, because it has been observed that organisms involved in metal redox cycling tend to have an abundance of these genes (e.g. 111 in *Geobacter sulfurreducens* and 42 in *Shewanella oneidensis*) (42, 43). Some of our MAGs were comparably rich in *c*-type cytochromes, including some MHCs with up to 7 CxxCH motifs. One MAG of the Chitinophagaceae had 52 cytochromes, the largest with 7 heme binding domains; and one MAG of the Armatimonadota had 48 cytochromes, the largest with 5 heme binding domains. Our Chroococcidiopsiaceae MAGs were fairly rich in cytochromes as well—the 4 Chroococcidiopsiaceae MAGs with > 93% completeness had 32, 32, 41, and 44 cytochrome genes, respectively.

Other known modes of microbial manganese oxidation use extracellular or outer membrane multicopper oxidase (MCO) enzymes to catalyze manganese oxidation (Fig. S8*E*) (44). This reaction is not coupled to metabolic energy conservation, and therefore does not require a mechanism of EET. A hypothetical porin-MCO complex has been proposed, suggested to function similarly to the porin-MHC complexes known to engage in EET, but currently lacks experimental support (Fig. S8*F*) (32). This hypothetical system is homologous to PcoAB, a periplasmic copper detoxification system. We specifically screened for MnxG (*Pseudomonas putida* GB-1) (45), CotA (*Bacillus pumilus* WH4) (46), MoxA (*Pedomicrobium* sp. ACM 3067) (47), McoA (*Pseudomonas putida* GB-1) (45), and MofA (*Leptothrix discophora*, with high homology to OmpB from *Geobacter sulfurreducens*), as MCOs implicated in manganese oxidation, along with PcoAB; we also screened for MCOs more generally, as determined by cupredoxin domains annotated in KBase. We identified MoxA, a protein known to exhibit manganese oxidation and laccase activity, in 5 of our MAGs, and PcoAB in two of them. Other MCOs are present in many of our MAGs (including 5 of the 6 Chroococcidiopsiaceae MAGs),

but given the catalytic breadth of this diverse family of enzymes, we hesitated to draw definitive conclusions about their specific functions based on genomic data alone.

The Cyanobacteria provide an additional mechanism for manganese oxidation that has not previously been discussed in the context of varnish—photosystem II oxidizes manganese (Fig. S8*G*), as exemplified by the photoassembly of the Mn_4CaO_5 cluster that enables water oxidation (48). There are several lines of evidence that oxygenic photosynthesis evolved in the ancestors of the Cyanobacteria from a version of anoxygenic photosynthesis based on manganese oxidation (49, 50), and it is possible this metabolism still exists in their modern decedents. Oxygenic phototrophs are often thought of as having an unlimited electron donor for photosynthesis, but under arid conditions water is scarce, and maintaining the ability to use manganese as an alternative electron donor might be useful. Thus, we propose an additional potential function for cyanobacterial manganese accumulation, particularly in the extremophilic, desiccation-resistant *Chroococcidiopsis*: these taxa might stockpile an electron reservoir to enable photosynthetic electron transport without using up water. This, along with the observations of a H-Mn^{2+} antioxidant system, suggests two potential physiological reasons that extreme manganese accumulation could be a useful ecological strategy for cyanobacterial survival in the arid, oxidizing environments where varnish forms.

C. Mn^{2+} speciation probed by paramagnetic resonance techniques

The EPR spectra of H-Mn^{2+} complexes discussed here are characteristic of an S = 5/2 ion with small zero-field splitting (ZFS), with the principal ZFS parameter, D, much less than the microwave quantum (hν) (51). Such spectra show a central ^{55}Mn (I = 5/2) sextet arising from hyperfine interactions, A ~ 90 G, that is associated with transitions between the m_s = +1/2 and

296 −1/2 electron-spin substates. These features ride on, and are flanked by, significantly broader
297 wings—signals from the four satellite transitions involving the other electron-spin substates (m_s
298 $\pm5/2 \Leftrightarrow \pm3/2$; $\pm3/2 \Leftrightarrow \pm1/2$). The net absorption spectrum is the sum of the five envelopes of
299 these five transitions among substates. The cellular Mn^{2+} EPR spectra of all Cyanobacteria
300 showed a resolved six-line ^{55}Mn hyperfine pattern centered at g-2 (~12 kG) riding on relatively
301 narrow wings extending to both high and low magnetic field with a total field span of 4 kG,
302 features which are suppressed in the derivative-mode CW EPR spectra (Fig. 3*B*). Frozen
303 standard solutions of Mn^{2+} complexed with orthophosphate, polyphosphate, and bicarbonate
304 show similar high-symmetry EPR spectra with relatively narrow wings (Fig. S10*A*). Much
305 broader wings are seen in low-symmetry complexes with chelating ligands (such as EDTA) and
306 proteins (such as MnSOD) (Fig. S10*A*-*B*).
307 The frozen solution ENDOR spectrum of an I = 1/2 nucleus, such as ^{31}P, ^{13}C, ^{1}H, coupled
308 to S = 5/2 Mn^{2+} comprises a set of doublets centered at the nuclear Larmor frequency, each split
309 by a multiple of the electron-nuclear hyperfine coupling (A). The primary doublet is associated
310 with the $m_s = \pm1/2$ electron spin sublevels of Mn^{2+} and is split by A; weaker satellite doublets
311 associated with the $m_s = \pm3/2$ and $\pm5/2$ sublevels are split by 3A and 5A. All spectra in this study
312 displayed ^{1}H signals that could be assigned to the protons of bound water (Fig. 3*C*). For a
313 phosphate moiety bound to a Mn^{2+} center we focused on the sharp $m_s = \pm1/2$ ^{31}P doublet. The
314 relative intensities of ^{31}P and ^{1}H signals provided a means of assessing Mn^{2+} speciation (52).
315 A ^{14}N nucleus (I = 1) directly coordinated with Mn^{2+} creates modulation in the electron spin echo
316 decay, which is dominated by ^{14}N hyperfine interaction (53). To quantitate ^{14}N ESEEM
317 responses from cellular Mn^{2+}, we chose as a standard the ^{14}N response from the Mn-imidazole
318 complex, which binds one imidazole and (presumably) five waters. Mn-imidazole showed a

strong time dependent modulation signal; no such signal was observed in any of the cyanobacterial samples (Fig. S10*C*). The absence of such a signal indicated that manganese resides in locations without a significant pool of nitrogenous ligands.

D. Cell biological insights suggest the cyanobacterial Mn^{2+} pool is periplasmic

The massive pool of manganese that we observed to accumulate in cyanobacterial cells is unlikely to be either cytoplasmic or extracellular. In the cytoplasm, where the cyanobacterial carbon concentrating mechanism accumulates substantial HCO_3^- (54), such a high abundance of Mn^{2+} would precipitate $MnCO_3$ minerals. Furthermore, the cytoplasm contains polyphosphate granules, which have a high affinity for Mn^{2+} (55–58). We did not observe such minerals, nor any manganese complexed by phosphates, in any of the cyanobacterial strains we examined. The manganese speciation that we did see— manganese complexed by small organic acids—is unlikely to be extracellular. Thus, we concluded that this manganese pool is most likely periplasmic.

Building on this is another line of evidence; this manganese pool cannot be disrupted by a vigorous water wash, supporting the interpretation that it is intra rather than extracellular. However, ~80% of it can be extracted with an EDTA wash, which is consistent with a periplasmic pool but not a cytoplasmic pool (59). Furthermore, a transporter that keeps manganese in the periplasm rather than the cytoplasm is known to be an essential aspect of manganese homeostasis in Cyanobacteria (60).

E. Relevance to Mars and astrobiological implications

Many previous studies have highlighted the resemblance of varnish to phenomena observed on Mars (9, 17). However, while many dark, shiny rocks have been observed on Mars, these are largely ventifacted rather than coated. Varnish itself (defined as a mixture of manganese and iron oxides and clay minerals) has not been definitively identified on Mars, and indeed only one instance of a potentially high- manganese surface coating has been found (61). The definitive manganese oxide phases that have been discovered on Mars do not appear to be associated with surface exposures, rather they precipitated in the subsurface (62). Therefore, we hesitate to assert any strong astrobiological interpretations for biological processes underpinning terrestrial varnish.

Supplemental References

1. R. S. Perry, J. B. Adams, Desert varnish: evidence for cyclic deposition of manganese. *Nature* **276**, 489–491 (1978).

2. D. Krinsley, Models of rock varnish formation constrained by high resolution transmission electron microscopy. *Sedimentology* **45**, 711–725 (1998).

3. L. A. J. Garvie, D. M. Burt, P. R. Buseck, Nanometer-scale complexity, growth, and diagenesis in desert varnish. *Geology* **36**, 215 (2008).

4. N. Thiagarajan, C.-T. Aeolus Lee, Trace-element evidence for the origin of desert varnish by direct aqueous atmospheric deposition. *Earth Planet. Sci. Lett.* **224**, 131–141 (2004).

5. M. Fleisher, T. Liu, W. S. Broecker, W. Moore, A clue regarding the origin of rock varnish. *Geophys. Res. Lett.* **26**, 103–106 (1999).

6. H. Bao, G. M. Michalski, M. H. Thiemens, Sulfate oxygen-17 anomalies in desert varnishes. *Geochim. Cosmochim. Acta* **65**, 2029–2036 (2001).

7. Y. Goldsmith, M. Stein, Y. Enzel, From dust to varnish: Geochemical constraints on rock varnish formation in the Negev Desert, Israel. *Geochim. Cosmochim. Acta* **126**, 97–111 (2014).

8. R. S. Perry, *et al.*, Baking black opal in the desert sun: The importance of silica in desert varnish. *Geology* **34**, 537 (2006).

9. R. S. Perry, V. M. Kolb, From Darwin to Mars: desert varnish as a model for preservation of complex (bio)chemical systems in R. B. Hoover, A. Y. Rozanov, Eds. (2004), pp. 136–144.

10. D. E. Northup, *et al.*, Diversity of rock varnish bacterial communities from Black Canyon, New Mexico. *J. Geophys. Res. Biogeosciences* **115**, G02007 (2010).

11. F. E. Palmer, J. T. Staley, R. G. E. Murray, T. Counsell, J. B. Adams, Identification of manganese-oxidizing bacteria from desert varnish. *Geomicrobiol. J.* **4**, 343–360 (1986).

12. K. R. Kuhlman, *et al.*, Diversity of Microorganisms within Rock Varnish in the Whipple Mountains, California. *Appl. Environ. Microbiol.* **72**, 1708–1715 (2006).

13. K. R. Kuhlman, P. Venkat, M. T. La Duc, G. M. Kuhlman, C. P. McKay, Evidence of a microbial community associated with rock varnish at Yungay, Atacama Desert, Chile. *J. Geophys. Res. Biogeosciences* **113** (2008).

14. N. Lang-Yona, *et al.*, Insights into microbial involvement in desert varnish formation retrieved from metagenomic analysis: The desert varnish microbiome. *Environ. Microbiol. Rep.* **10**, 264–271 (2018).

15. A. Esposito, *et al.*, Comparison of Rock Varnish Bacterial Communities with Surrounding Non-Varnished Rock Surfaces: Taxon-Specific Analysis and Morphological Description. *Microb. Ecol.* **70**, 741–750 (2015).

16. A. Esposito, L. Borruso, J. E. Rattray, L. Brusetti, E. Ahmed, Taxonomic and functional insights into rock varnish microbiome using shotgun metagenomics. *FEMS Microbiol. Ecol.* **95**, fiz180 (2019).

17. D. Krinsley, R. I. Dorn, B. DiGregorio, Astrobiological Implications of Rock Varnish in Tibet. *Astrobiology* **9**, 551–562 (2009).

18. R. I. Dorn, “Rock Varnish” in *Geochemical Sediments & Landscapes*, (Blackwell, 2007), pp. 246–297.

19. W. E. Krumbein, Über den Einfluß der Mikroflora auf die exogene Dynamik (Verwitterung und Krustenbildung). *Geol. Rundsch.* **58**, 333–363 (1968).

20. G. Grote, W. E. Krumbein, Microbial precipitation of manganese by bacteria and fungi from desert rock and rock varnish. *Geomicrobiol. J.* **10**, 49–57 (1992).

21. R. I. Dorn, T. M. Oberlander, Microbial Origin of Desert Varnish. *Science* **213**, 1245–1247 (1981).

22. B. Hungate, *et al.*, Characterization of manganese-oxidizing (MnII→MnIV) bacteria from Negev Desert rock varnish: implications in desert varnish formation. *Can. J. Microbiol.* **33**, 939–943 (1987).

23. B. M. Tebo, *et al.*, Biogenic Manganese Oxides: Properties and Mechanisms of Formation. *Annu. Rev. Earth Planet. Sci.* **32**, 287–328 (2004).

24. C. M. Hansel, C. A. Zeiner, C. M. Santelli, S. M. Webb, Mn(II) oxidation by an ascomycete fungus is linked to superoxide production during asexual reproduction. *Proc. Natl. Acad. Sci. U. S. A.* **109**, 12621–12625 (2012).

25. N. Miyata, Y. Tani, K. Iwahori, M. Soma, Enzymatic formation of manganese oxides by an Acremonium-like hyphomycete fungus, strain KR21-2. *FEMS Microbiol. Ecol.* **47**, 101–109 (2004).

26. K. J. Parchert, M. N. Spilde, A. Porras-Alfaro, A. M. Nyberg, D. E. Northup, Fungal Communities Associated with Rock Varnish in Black Canyon, New Mexico: Casual Inhabitants or Essential Partners? *Geomicrobiol. J.* **29**, 752–766 (2012).

27. J. J. Morgan, Kinetics of reaction between O2 and Mn(II) species in aqueous solutions. *Geochim. Cosmochim. Acta* **69**, 35–48 (2005).

28. X. Xu, *et al.*, Characteristics of desert varnish from nanometer to micrometer scale: A photo-oxidation model on its formation. *Chem. Geol.* **522**, 55–70 (2019).

29. D. H. Krinsley, B. DiGregorio, R. I. Dorn, J. Razink, R. Fisher, Mn-Fe-Enhancing Budding Bacteria in Century-Old Rock Varnish, Erie Barge Canal, New York. *J. Geol.* **125**, 317–336 (2017).

30. M. Bergkessel, D. W. Basta, D. K. Newman, The physiology of growth arrest: uniting molecular and environmental microbiology. *Nat. Rev. Microbiol.* **14**, 549–562 (2016).

31. D. J. Richardson, *et al.*, The "porin-cytochrome" model for microbe-to-mineral electron transfer. *Mol. Microbiol.* **85**, 201–212 (2012).

32. S. He, R. A. Barco, D. Emerson, E. E. Roden, Comparative Genomic Analysis of Neutrophilic Iron(II) Oxidizer Genomes for Candidate Genes in Extracellular Electron Transfer. *Front. Microbiol.* **8**, 1584 (2017).

33. H. Yu, J. R. Leadbetter, Bacterial chemolithoautotrophy via manganese oxidation. *Nature* **583**, 453–458 (2020).

34. A. S. Beliaev, D. A. Saffarini, Shewanella putrefaciens mtrB encodes an outer membrane protein required for Fe(III) and Mn(IV) reduction. *J. Bacteriol.* **180**, 6292–6297 (1998).

35. J. Liu, *et al.*, Identification and Characterization of MtoA: A Decaheme c-Type Cytochrome of the Neutrophilic Fe(II)-Oxidizing Bacterium Sideroxydans lithotrophicus ES-1. *Front. Microbiol.* **3**, 37 (2012).

36. Y. Jiao, D. K. Newman, The pio operon is essential for phototrophic Fe(II) oxidation in Rhodopseudomonas palustris TIE-1. *J. Bacteriol.* **189**, 1765–1773 (2007).

37. J. J. Lamb, M. F. Hohmann-Marriott, Manganese acquisition is facilitated by PilA in the cyanobacterium Synechocystis sp. PCC 6803. *PLOS ONE* **12**, e0184685 (2017).

38. F. Wang, *et al.*, Structure of Microbial Nanowires Reveals Stacked Hemes that Transport Electrons over Micrometers. *Cell* **177**, 361-369.e10 (2019).

39. C. Castelle, *et al.*, A New Iron-oxidizing/O_2-reducing Supercomplex Spanning Both Inner and Outer Membranes, Isolated from the Extreme Acidophile *Acidithiobacillus ferrooxidans*. *J. Biol. Chem.* **283**, 25803–25811 (2008).

40. C. Jeans, *et al.*, Cytochrome 572 is a conspicuous membrane protein with iron oxidation activity purified directly from a natural acidophilic microbial community. *ISME J.* **2**, 542–550 (2008).

41. R. A. Barco, *et al.*, New Insight into Microbial Iron Oxidation as Revealed by the Proteomic Profile of an Obligate Iron-Oxidizing Chemolithoautotroph. *Appl. Environ. Microbiol.* **81**, 5927–5937 (2015).

42. T. E. Meyer, *et al.*, Identification of 42 Possible Cytochrome C Genes in the *Shewanella oneidensis* Genome and Characterization of Six Soluble Cytochromes. *OMICS J. Integr. Biol.* **8**, 57–77 (2004).

43. B. A. Methe, Genome of Geobacter sulfurreducens: Metal Reduction in Subsurface Environments. *Science* **302**, 1967–1969 (2003).

44. A. V. Soldatova, *et al.*, Mn(II) oxidation by the multicopper oxidase complex Mnx: A coordinated two-stage Mn(II)/(III) and Mn(III)/(IV) mechanism. *J. Am. Chem. Soc.* (2017) https:/doi.org/10.1021/jacs.7b02772.

45. K. Geszvain, J. K. McCarthy, B. M. Tebo, Elimination of Manganese(II,III) Oxidation in Pseudomonas putida GB-1 by a Double Knockout of Two Putative Multicopper Oxidase Genes. *Appl. Environ. Microbiol.* **79**, 357–366 (2013).

46. J. Su, *et al.*, CotA, a Multicopper Oxidase from Bacillus pumilus WH4, Exhibits Manganese-Oxidase Activity. *PLoS ONE* **8**, e60573 (2013).

47. J. P. Ridge, *et al.*, A multicopper oxidase is essential for manganese oxidation and laccase-like activity in Pedomicrobium sp. ACM 3067. *Environ. Microbiol.* **9**, 944–953 (2007).

48. H. Bao, R. L. Burnap, Photoactivation: The Light-Driven Assembly of the Water Oxidation Complex of Photosystem II. *Front. Plant Sci.* **7** (2016).

49. J. E. Johnson, *et al.*, Manganese-oxidizing photosynthesis before the rise of cyanobacteria. **110**, 11238–11243 (2013).

50. W. W. Fischer, J. Hemp, J. E. Johnson, Manganese and the Evolution of Photosynthesis. *Orig. Life Evol. Biosphere J. Int. Soc. Study Orig. Life* **45**, 351–357 (2015).

51. A. Sharma, *et al.*, Responses of Mn2+ speciation in Deinococcus radiodurans and Escherichia coli to -radiation by advanced paramagnetic resonance methods. *Proc. Natl. Acad. Sci.* **110**, 5945–5950 (2013).

52. R. L. McNaughton, *et al.*, Probing in vivo Mn2+ speciation and oxidative stress resistance in yeast cells with electron-nuclear double resonance spectroscopy. *Proc. Natl. Acad. Sci. U. S. A.* **107**, 15335–15339 (2010).

53. K. M. Salikhov, Schweiger, A., Jeschke, G.:Principles of pulse electron paramagnetic resonance: XXVI, 478 pp. Oxford University Press, Oxford 2001. Hardcover GBP 95.00. *Appl. Magn. Reson.* **22**, 319–319 (2002).

54. N. M. Mangan, A. Flamholz, R. D. Hood, R. Milo, D. F. Savage, pH determines the energetic efficiency of the cyanobacterial CO_2 concentrating mechanism. *Proc. Natl. Acad. Sci.* **113**, E5354–E5362 (2016).

55. M. Tsednee, *et al.*, Manganese co-localizes with calcium and phosphorus in *Chlamydomonas* acidocalcisomes and is mobilized in manganese-deficient conditions. *J. Biol. Chem.* **294**, 17626–17641 (2019).

56. R. Docampo, "Acidocalcisomes and Polyphosphate Granules" in *Inclusions in Prokaryotes*, Microbiology Monographs., J. M. Shively, Ed. (Springer-Verlag, 2006), pp. 53–70.

57. S. P. Santos, *et al.*, The interplay between Mn and Fe in Deinococcus radiodurans triggers cellular protection during paraquat-induced oxidative stress. *Sci. Rep.* **9**, 17217 (2019).

58. M. Hauck, Effects of manganese on the viability of vegetative diaspores of the epiphytic lichen Hypogymnia physodes. *Environ. Exp. Bot.* **47**, 127–142 (2002).

59. N. Keren, M. J. Kidd, J. E. Penner-Hahn, H. B. Pakrasi, A light-dependent mechanism for massive accumulation of manganese in the photosynthetic bacterium Synechocystis sp. PCC 6803. *Biochemistry* **41**, 15085–15092 (2002).

60. F. Brandenburg, *et al.*, The *Synechocystis* Manganese Exporter Mnx Is Essential for Manganese Homeostasis in Cyanobacteria. *Plant Physiol.* **173**, 1798–1810 (2017).

61. N. L. Lanza, *et al.*, High manganese concentrations in rocks at Gale crater, Mars. *Geophys. Res. Lett.* **41**, 5755–5763 (2014).

62. N. L. Lanza, *et al.*, Oxidation of manganese in an ancient aquifer, Kimberley formation, Gale crater, Mars: Manganese Fracture Fills in Gale Crater. *Geophys. Res. Lett.* **43**, 7398–7407 (2016).